

Spectrally and spatially resolved cathodoluminescence of undoped/Mg-doped GaN core-shell nanowires: a local probe into activation of Mg acceptors in non-polar and semi-polar crystal faces

V. Hortelano^{1,*}, O. Martínez¹, L. Artús², R. Cuscó², and J. Jiménez¹

¹*GdS Optronlab, ed.i+d, Paseo de Belén 11, Universidad de Valladolid, 47011 Valladolid, Spain*

²*Institut Jaume Almera, ICTJA-CSIC, Consejo Superior de Investigaciones Científicas, 08028 Barcelona, Spain*

Abstract

Spectrally and spatially resolved cathodoluminescence (CL) measurements were carried out at 80 K on undoped/Mg-doped GaN core-shell nanowires grown by selective area growth metalorganic vapor phase epitaxy in order to investigate locally the optical activity of the Mg dopants. A study of the luminescence emission distribution over the different regions of the nanowires is presented. We have investigated the CL fingerprints of the Mg incorporation into the non-polar lateral prismatic facets and the semi-polar facets of the pyramidal tips. The amount of Mg incorporation/activation was varied by using several Mg/Ga flow ratios and post-growth annealing treatments. For lower Mg/Ga flow ratios, the annealed nanowires clearly display a donor-acceptor pair band emission peaking at 3.26-3.27 eV and up to 4 LO phonon replicas, which can be considered as a reliable indicator of effective p-type Mg doping in the nanowire shell. For higher Mg/Ga flow ratios, a substantial enhancement of the yellow luminescence emission as well as several emission subbands are observed, which suggests an increase of disorder and the presence of defects as a consequence of the excess Mg doping,

PACS numbers: 78.67.Uh, 78.60-Hk, 78.66.Fd

- Present address:
Humboldt-Universität zu Berlin
Institut für Physik
Newtonstr. 15
D-12489 Berlin, Germany

1. INTRODUCTION

In the last few years, GaN-based nanowires have attracted much interest as a possible route to overcome the intrinsic limitations of present-day GaN optoelectronics based on thin film (0001) GaN layers grown on foreign substrates. Whereas such layers exhibit a high dislocation density and spontaneous piezoelectric polarization, which are both detrimental to the performance and lifetime of the devices, GaN-based nanowires are basically free of threading dislocations as their high aspect ratio and small diameter allow for efficient strain relief by purely elastic mechanisms [1,2]. Additionally, the sidewall non-polar *m* facets of *c*-axis nanowires permit the growth of core-shell InGaN/GaN quantum wells that are not affected by the quantum Stark effect [3-6], and therefore are promising structures for high-efficiency light emitting device (LED) applications. Densely-packed self-organized nanowires have been shown to yield high quantum efficiency [2], constituting a real alternative to thin films. Nowadays, homogeneous arrays of nanowires can be obtained by selective-area growth (SAG). Because of the dramatic increase in active area, superior crystallinity, and enhanced light absorption and carrier collection [6], core-shell nanowire devices are expected to deliver a high throughput in solar cells and optoelectronic devices. For most of these applications it is essential to assess the homogeneity, not only of the shape, but also of the optical properties of the nanowires. The CL emission distribution at various regions across the nanowire can provide valuable information about doping efficiency and defect formation.

The achievement of effective p-type doping is a crucial issue for the development of optoelectronic devices. Substitutional Mg in Ga site is the acceptor that provides more efficient p-type doping in GaN [7-9]. Due to the high thermal activation energy of Mg acceptors (~ 200 meV), high Mg concentrations (close to the solubility limit) have to be added to reach suitable free-hole concentrations ($>10^{17}$ cm $^{-3}$). The incorporation of Mg as an acceptor depends on the III/V flow ratio, the nature of the precursors, the growth temperature, and the Mg precursor flow. On the other hand, the influence of the facets on the incorporation of the impurities into nanowires has been reported [10]. In spite of its great interest, the Mg doping of non-polar and semipolar GaN faces in SAG nanowires has been scarcely studied. Moreover, although the incorporation of Mg is crucial for optoelectronic devices, it is not easy to assess the effective doping level in reduced size structures because the electrical characterization techniques commonly used for this purpose [e.g. Hall Effect, or capacitance voltage (CV)] are difficult to apply to nanowires. Luminescence techniques provide an alternative tool to study the Mg incorporation into the GaN nanowires. In particular, spectrally resolved cathodoluminescence (CL) allows local emission spectra to be obtained with a much higher spatial resolution compared to other optical techniques such as micro-photoluminescence (PL). This makes CL a unique tool to characterize the Mg-doped GaN nanowires, since it enables the study of the possible differences in the Mg incorporation into the different growth facets as well as the homogeneity of the nanowires.

In this work, we present a CL study of Mg doping in the outer shell of core-shell GaN nanowires grown under different Mg/Ga flow ratios. The spatial distribution of the Mg-acceptor- and defect-related emissions throughout a single nanowire has been studied using monochromatic CL imaging and spectrally resolved CL analysis. These emissions are not evenly distributed over the volume of the nanowires. The emission trends observed in the nanowires provide an indication of the incorporation and activation of Mg acceptors in non-polar and semi-polar faces in nanowires grown by SAG under different Mg/Ga flow ratios.

II. EXPERIMENTAL AND SAMPLES

Highly uniform GaN nanowire arrays were grown by SAG in a metalorganic vapour-phase epitaxy (MOVPE) reactor using trimethyl gallium and ammonia as the precursors. The prismatic nanowires are undoped/Mg-doped GaN core-shell structures which exhibit non-polar m -plane lateral faces and are capped by a semipolar r -plane faceted hexagonal-pyramid tip. The samples consist of vertically-aligned, coaxial undoped/p-doped structures distributed over a close-packed hexagonal array. The Mg-doped nanowires were grown on GaN/sapphire templates with a SiN_x mask with submicrometer openings produced by nanoimprint lithography and dry etching. First, an undoped GaN core is formed, which is then laterally overgrown with a Mg-doped GaN layer. The sample characteristics are summarized in Table I. The Mg/Ga flow ratio was varied in order to introduce different amounts of Mg dopants. The nanowire dimensions given in Table I are average values of the sizes observed over different zones of the samples.

The Mg acceptor activation was performed in flowing N_2 at 700 °C for 15 min. Transmission electron microscopy measurements (TEM) were performed using a JEM 2200 (JEOL) electron microscope. The CL study was carried out with a MonoCL2 system from Gatan UK, attached to a field-emission scanning electron microscope (FESEM-LEO 1530). The detector for the spectral analysis was a Peltier-cooled CCD, while a photomultiplier tube was used for recording panchromatic and monochromatic CL images. The measurements were carried out at 80 K. The acceleration voltage of the e-beam was varied between 5 and 20 kV. The penetration depth in GaN at 5 kV is ≈ 150 nm, with maximum energy loss at around 50 nm, whereas the penetration depth at 20 kV is ≈ 1.5 μm , with maximum loss energy around 500 nm [11]. Therefore, using an acceleration voltage of 5 kV permits the outer p-type shell layer to be studied with minimal contribution of the nanowire core. Unless otherwise specified, all the spectra presented in this work were obtained at 5 kV. The samples were observed in top view with the as grown nanowires attached to the substrate, thus exposing the pyramidal tip. Some nanowires were scratched and deposited onto a lacey carbon grid for sidewall m -plane observation. The e-beam current was low enough to prevent low-energy electron-beam interaction (LEEBI) activation of the Mg acceptors [12]. In fact, we did not observe spectral changes under persistent e-beam exposure.

A. MORPHOLOGY

Top view SEM images of the nanowires for the as-grown samples are displayed in Fig. 1. These images show hexagonal cross section, in accordance with the wurtzite structure. The vertically aligned nanowires present a highly uniform cross sectional size. The cross sectional size depends on the patterned hole diameter in the template, the nanowire height, the pitch and the pattern orientation, which were the same for all the samples studied. The small differences in cross-sectional size observed in samples A to C cannot be attributed to the Mg doping, as similar differences are found between different regions of each sample, but might be related to the size of the nanowire core.

Scratched nanowires were used to obtain SEM sidewall images (Fig. 2). These images allow one to observe the prismatic sidewalls and the pyramidal-tip end of the nanowires, which was not truncated. As the pyramidal tip is not truncated, the (0001) polar planes are only exposed on the nanowire base of the scratched nanowires.

The outer Mg-doped shell is about 150-200 nm thick in the prismatic sidewalls (m planes) and around 25-30 nm thick in the pyramidal semi-polar faces (r planes). These differences in the Mg-doped shell thickness are consistent with the decreasing growth-rate trend for polar (0001), non-polar (1-100) and semi-polar (1-101) planes reported in Ref [13]. While as noted above, the Mg/Ga flow ratio does not seem to influence the cross sectional size, the height ratio between the prismatic base and the top pyramid seems to increase with the Mg flux, which suggests that the $\langle 0001 \rangle$ growth rate increases with Mg incorporation. Unlike Beaumont et al. [14], who reported truncated pyramidal morphology in Mg doped nanowires, we have not observed pyramid truncation in any of our core-shell nanowire structures

B. CATHODOLUMINESCENCE ANALYSIS OF THE NANOWIRES

The luminescence spectrum of Mg doped GaN depends on the amount of Mg incorporated [9,15]. In Fig. 3 we display a typical CL spectrum obtained at 80 K on one of the studied nanowires. For comparison, the CL spectrum of an undoped nanowire is also displayed. Three main spectral signatures in the CL spectrum of the Mg-doped nanowires can be distinguished. The near-band-edge emission (NBE) around 3.46 eV arises from donor-bound excitons. The characteristic spectral fingerprint of Mg-doped GaN is a multiline band peaking between 3.0 and 3.27 eV which arises from donor-acceptor pair (DAP) transitions involving Mg acceptors and shallow donors and their phonon replicas. The shape of this band greatly depends on the amount of Mg incorporated. The line-shape variations observed for different concentrations illustrate the complexity of the Mg acceptor configuration in the GaN lattice [9], and the difficulty to set up the conditions for the optimum Mg doping. Recently, different DAP transitions associated with three Mg-related acceptor levels have been reported [16]. The shape of the DAP band depends on the relative intensity of these three DAP transitions and it can substantially differ from a standard DAP peak with its corresponding phonon replicas. This band can appear even energetically shifted depending on the Mg concentration and the dominant DAP transition. Additionally, long-range potential fluctuations have been reported in Mg-doped GaN, which can also contribute to change the shape of the DAP band [9,17]. Finally, a broad yellow luminescence band (YL) related to deep levels is also present. This broad band, usually associated with V_{Ga} complexes, peaks at around 2.2 eV and it is generally present in GaN luminescence spectra [15]. The intensities of the three bands (NBE, DAP and YL band) in Mg doped GaN are interrelated. In particular, it is found that the YL band decreases with increasing DAP emission, which can be related to the decrease of V_{Ga} concentration in Mg doped GaN [18]. Regarding the NBE emission, its intensity has been reported to decrease with the incorporation of Mg acceptors [19,20].

Top view panchromatic images of the samples grown with different Mg/Ga flow ratios are shown in Fig. 4. Similar emission patterns are observed for different nanowires in a specific sample, which is consistent with the high morphological homogeneity observed in the SEM images of Fig. 1. One can assume that the Mg incorporation on the different nanowires of a sample follows the same pattern, being governed by the different crystal orientations and the Mg/Ga flow ratio. The panchromatic image of an undoped sample is also shown in Fig. 4 (d) for comparison.

These images reveal the luminescence emission pattern in the semipolar planes and at the prism/pyramid (m - r) edge. The panchromatic images show dark contrast at the pyramid apex. By comparing the dark area around the pyramid apex in Fig. 4 (c) with the analogous region in Fig. 4 (a), we can see that the contrast of the dark area increases with the Mg/Ga flow ratio. A bright belt around the dark contrasted apex area is observed in the lower part of the pyramidal facets for all the samples, but it displays marked differences between them.

The width of the bright belt decreases for increasing Mg/Ga flow ratio as a consequence of the progressive broadening of the dark m - r edge. This dark edge is barely a narrow line in the nanowires grown with the lowest Mg flow [Fig. 4 (a)], and it is fully absent in the undoped reference sample [Fig. 4 (d)]. This variation of the dark contrast at the m - r edge suggests that it is related to non-radiative recombination centers (NRRCs) created by the incorporation of Mg, since it is well known that Mg doping can introduce structural defects [21]. Line-scan profiles of the panchromatic CL intensities across the nanowires for the as-grown samples are shown in Fig. 5. One can observe the progressive extension of the dark areas at the m - r edges as the Mg/Ga flow ratio increases. In particular, an incipient suppression of the CL emission can be clearly noticed in the m - r edge of sample B, which evolves towards a pronounced suppression in sample C. The dark contrast at the m - r edge and at the apex is also present in the Mg-doped samples after annealing, as can be seen in the panchromatic CL images of the annealed samples shown in Fig. 6.

While the dark contrast in the m - r edges is absent in undoped nanowires, the apex still appears dark-contrasted in undoped nanowires, which suggests the formation of NRRCs at the apex independently of the Mg doping. Figure 7 displays TEM images of the pyramid apex in sample A showing the different orientation of the crystal planes. Regarding the m - r edges, it seems that Mg incorporation plays a significant role in the formation of NRRCs around those edges. The formation of stacking faults (SFs), pyramidal inversion domains (PIDs), twins and other structural defects has been reported in c -plane Mg-doped GaN films grown by metal-organic chemical vapour deposition (MOCVD) [21] and also in self-assembled Mg-doped GaN nanowires grown by plasma-assisted molecular beam epitaxy [23]. SFs have been reported to be optically active in some cases, emitting at three characteristic bands at 3.29, 3.33 and 3.41 eV [21]. However, CL studies on homoepitaxially grown m -plane Mg-doped GaN layers with a high density of SFs showed insignificant emission of these bands [22]. We have not detected emission from the characteristic SF related bands in the m - r edges of our core-shell nanowire samples.

To investigate the emission distribution in non-polar m planes, some nanowires were scratched and CL images were taken from the sidewalls. The panchromatic CL images are shown in Fig. 8. For sample A, bright m planes and dark edges between them are observed. For sample B, the emission from the bright belt around the pyramidal tip appears as intense as the emission from the m planes. The bright belt emission is even more marked for the highest Mg/Ga flow ratio (sample C), where it looks brighter than the prismatic non-polar faces, although it is narrower than in nanowires grown with lower Mg/Ga flow ratios. The dark edges observed between m faces can be associated with the existence of dislocations. In fact, as can be seen in Fig. 9, TEM measurements reveal the presence of dislocations at the edge between two prismatic m faces.

III. DISCUSSION

The panchromatic images contain the contribution of the overall luminescence emission within the detector spectral range (300-900 nm). In order to study the distribution of the different CL emissions, monochromatic CL images were recorded for the NBE, DAP and YL emissions. Figure 10 shows monochromatic CL images of two nanowires from the annealed sample A. These images illustrate the locations in the nanowires which yield the different emissions. One of the nanowires is inverted exposing the base, while the other is lying down exposing the sidewalls. The monochromatic image of the DAP emission shows that it primarily arises from the nanowire outer shell (notice the O-ring like emission pattern in the base of the inverted nanowire). The DAP emission is sharply quenched around the apex

and also along the edges, while the YL band is mainly localized in the nanowire core and in the pyramid apex, and is almost unappreciable in the non-polar faces. In contrast, the NBE emission intensity is highest in the nanowire core, particularly in the semipolar pyramidal faces in the region close to the apex. Note that the image of the semi-polar planes might contain also some contribution from the nanowire core because the thickness of the Mg-doped shell in those facets (~30 nm) is slightly lower than the CL probing depth at 5 kV. On the other hand, from the monochromatic images of Fig. 10, it can be seen that the bright belt around the pyramidal tip observed in the panchromatic CL images of Figs. 4 and 7 is clearly associated with the DAP emission.

The distribution of the different luminescence bands provides interesting hints about the location of Mg acceptors in the nanowires. The fingerprint of substitutional Mg in the luminescence spectrum of GaN is the DAP transition. The spectral shape of the DAP luminescence band is strongly dependent on the concentration of electrically activated Mg acceptors. PL spectra with the DAP band peaking at 3.26-3.27 eV together with the corresponding phonon replicas and the suppression of the YL band were reported by Y. P. Sui *et al.* [20] in MOCVD-grown Mg-doped GaN samples with high hole concentration. On the other hand, it is well known that the incorporation of high concentrations of Mg can degrade the crystal quality. For example, PIDs, which degrade the optical yield of GaN devices, have been reported to occur in heavily Mg-doped GaN films [24]. In order to optimize the Mg doping, it is desirable to have spectral criteria that allow us to assess the degree of Mg doping and activation achieved. To this aim, the CL spectral analysis of individual nanowires can be a useful tool for checking the incorporation and the activation of Mg acceptors in the nanowires under different growth and annealing conditions.

Local spectra were acquired on different facets of individual nanowires. In Fig 11 we show representative CL spectra of single nanowires from the as-grown and annealed samples A to C, both for non-polar and semi-polar faces. As can be seen in the panchromatic image displayed in Fig. 4, the overall CL emission features a high homogeneity over the nanowire ensemble in a given sample. However, the study of individual nanowires reveals local changes in the CL intensity and spectral distribution depending on the probed zone of the nanowire (see Fig. 10). The CL spectra of individual nanowires give information about the local characteristics of the nanowire luminescence which cannot be provided by the spectra recorded with optical techniques that use larger probe sizes, such as micro-PL, or directly from the panchromatic CL images discussed above. The CL spectra of the as-grown samples, both for the non-polar and the semi-polar faces, are shown in Figs. 11 (a) and (b), respectively. It can be seen that the CL spectra present different features on the three samples and the two faces studied, and that the structure of the multiline DAP emission depends on both the Mg/Ga flow ratio and the crystal face. The CL intensity of the DAP band decreases with increasing Mg/Ga flow ratio in the as-grown samples, both in *m* and *r* faces, which suggests that the concentration of NRRCs increases with the incorporation of Mg.

After annealing, when the Mg acceptors are expected to be activated, an increase of the DAP emission can be observed in all of the three samples, together with a decrease of the NBE and YL band emissions. The DAP emission enhancement is higher in sample A. The comparison between the absolute emission intensities of *m* and *r* faces is not straightforward because of the different thickness of the Mg doped layer in each face.

Although it is well known that H tends to form inactive complexes during MOCVD growth of Mg-doped GaN [15], further studies revealed that other substitutional/interstitial Mg complexes, as those theoretically predicted in [25], may also contribute to passivate the acceptors. As it can be seen in Fig. 11, when the Mg concentration is increased, the DAP band broadens and redshifts. The CL emission peak at around 3.16 eV dominates the DAP band in the sample with the highest Mg concentration (sample C), whereas for the lowest Mg

concentration (sample A), a subband peaking at 3.26-3.27 eV has a stronger contribution to the DAP band. It has been claimed that by increasing the Mg concentration, a broad blue band peaking at 2.8-3 eV develops in Mg-doped GaN, arising from transitions between deep donor levels and Mg acceptors [9,15]. However, none of our samples exhibited a dominant blue emission, which suggests that the Mg concentration does not exceed 10^{20} cm^{-3} in our samples [26]. The as-grown nanowires present a partial activation of the Mg acceptors, as indicated by the presence of the DAP bands, likely due to Mg-related levels activated during the post-growth cooling [27]. The DAP contribution appears more intense for the lower Mg/Ga flow ratio (sample A), which implies an increase of the Mg_{Ga} acceptors available. By comparing the CL spectra obtained on *r* and *m* faces of as-grown samples, it can be seen that the spectra on the *r* face of samples A and B look similar to the spectra on the *m* face of samples B and C, respectively [see Figs. 11 (a) and (b)]. This observation points to a higher Mg incorporation into *r* faces with respect to *m* faces. However, higher overall Mg incorporation does not necessarily imply more efficient p-type doping since other compensating/passivating defects can be created in the incorporation process. The complex structure of the DAP band at high Mg doping concentrations can be explained by potential fluctuations that occur in highly-compensated or heavily-doped material [9,17] and by the existence of several Mg-related DAP transitions involving either different Mg-acceptor levels or different donors [8,16]. Also, the appearance of cubic phases as Mg doping is increased has been proposed as the origin of the 3.16 eV band, which is dominant in heavily Mg-doped GaN[28]. The YL band has been reported to occur in n-type and semi-insulating Mg-doped GaN [15,29,30]. However, it was severely suppressed in p-type Mg-doped GaN [15,21], which was attributed to the reduction of the V_{Ga} defect concentration because of the formation of substitutional Mg_{Ga} . It should be noted that the strong reduction in the intensity of the YL band after annealing supports its V_{Ga} origin instead of other possible origins, such as residual C impurities [15]. The comparison between the Mg-related DAP emission and the intensity of the YL band can provide a more reliable assessment of the actual acceptor activation in GaN nanowires. Therefore, the observation of a DAP band peaking at 3.26-3.27 eV and the associated phonon replicas together with the simultaneous reduction of the YL band emission can be considered reliable fingerprints for the effective p-type Mg doping of the nanowires [15,22]. These results are consistent with a previous study of the PL spectra and the free-hole concentration in MOCVD-grown Mg-doped GaN [20], where it was found that the samples with highest hole concentration display a spectrum with the DAP band peaking at 3.26-3.27 eV together with the corresponding phonon replicas and the suppression of the YL band. The above analysis of the DAP and YL bands can therefore be a useful criterion for assessing the effective Mg doping in the GaN nanowires.

The annealing of Mg-doped GaN favors p-type doping activation by removing the passivation induced by H, which tends to form inactive complexes during MOCVD growth [15]. The CL spectra taken on non-polar and semipolar faces of the three annealed samples are shown in Figs. 11 (c) and (d), respectively. It can be seen that, as a consequence of the Mg-acceptor activation, the DAP emission is enhanced after annealing in all of the samples, and a concomitant reduction of the NBE and YL band emissions takes place. In Fig. 12 detailed spectra of the DAP bands recorded from a non-polar *m* face of sample A before and after annealing are displayed (curves b and a, respectively). The DAP band of an annealed sample having a higher Mg concentration (sample B) is also shown for comparison (curve c). As can be seen in this figure, the DAP band of the annealed sample A presents a peak emission at 3.26-3.27 eV and a regular series of bands separated each other by 92 meV intervals (energy of the LO phonon) which correspond to the LO phonon replicas. These replicas are not observed in the spectrum of the as-grown sample (curve b of Fig 12), nor in the spectra of samples grown with higher Mg/Ga flow, even after annealing, as illustrated by

curve c of Fig. 12). Then, the absence of clear phonon replica series and the appearance of several emission subbands in the DAP emission, as seen in spectra b and c of Fig. 12, suggest the existence of different transitions and/or potential fluctuations in these samples. It has been recently claimed that the DAP band appears redshifted in compensated Mg-doped GaN layers [20]. As explained above, the changes in the shape of the DAP multiline-band points out to the existence of disorder and compensating defects as a consequence of the excess of Mg doping [8,9,15,22]. This issue is of the highest relevance since it has been reported that for Mg concentrations above an upper threshold $\sim 2 \times 10^{19} \text{ cm}^{-3}$, self-compensation reduces the hole density, and maximum free hole concentrations of about $2 \times 10^{18} \text{ cm}^{-3}$ have been reported [31]. Among the GaN nanowires doped with different Mg fluxes used in this study, our CL measurements show that the annealed nanowires grown with a Mg/Ga flux ratio of 1.4 are those which more clearly display a DAP band emission peaking at around 3.26-3.27 eV with the corresponding phonon replicas up to third or fourth order. Further research is required to establish a precise correlation between the structure of the DAP transitions and the activation of holes in Mg-doped GaN, which could be advantageously used as a versatile tool for studying the Mg-doping effectiveness in GaN-based nanostructures.

The dependence on the Mg/Ga flow ratio of the DAP and YL band intensities normalized to the total emission is shown in Fig 13, both for non-polar and semipolar faces of as-grown and annealed samples. The graphs illustrate the anticorrelation between DAP and YL bands in all cases, as well as the intensity enhancement of the DAP emission and the decrease of the YL emission after annealing. This behaviour, in conjunction with the changes that occur in the structure of the DAP band discussed above, suggests that the activation is not merely due to the removal of passivating H in the Mg-H bonds, but is also a consequence of the redistribution of the Mg impurities and defects. Regarding the dependence of the DAP band intensity on the Mg flow, Fig 13 shows that both for *m* and *r* faces the maximum intensity of the DAP band is obtained after annealing in the samples grown with a Mg/Ga flow ratio of 1.4. Concurrently, these samples also display the lowest intensity of the YL band. As already mentioned, the comparison between the intensities arising from the *m* and *r* faces is not straightforward since the p-doped shell thickness is higher in the non-polar prismatic faces than in the semipolar pyramidal facets. Nevertheless, it can be clearly deduced from these graphs that the role of Mg flux and the post-growth annealing process prevails over that of the face orientation in achieving an effective p-type doping of the Mg-doped GaN nanowires studied in this work.

Top view spectral images have been acquired for individual nanowires. The intensity distributions of the DAP and the YL bands normalized to the total CL emission are shown in Figs. 14 and 15 for separate nanowires obtained from the annealed samples A and B, respectively. Local CL spectra acquired at the apex, the bright belt, and the *m-r* edge are also compared with a spectrum taken on the non-polar *m* face in Figs. 14 (d) and 15 (d).

For sample A, the spectral features discussed above in relation to the DAP transitions are observed in the CL spectra obtained at the three selected points [see Figs. 14 (b) and 14 (d)]. The non-polar *m* face presents a CL spectrum with a maximum at 3.26-3.27 eV and the associated phonon replicas, while the semipolar face (point 3) exhibits a slightly different DAP shape which may arise due to different transition probabilities between the donor and acceptor levels involved in the DAP transitions. On the other hand, the DAP emission decreases substantially in the *m-r* edge and in the apex, and its shape differs from those observed in the non-polar and semipolar faces.

A different distribution of the DAP emission is found in sample B [see Figs. 15 (b) and 15 (d)]. The dark *m-r* edge is well defined and broadened with respect to sample A, in agreement with the results shown in Figs. 5- 7. By comparing Figs. 14 (b) and 15 (b), it can be seen that the bright belt in the semipolar faces around the tip is narrowed with respect to

the one observed in sample A, as a consequence of a different NRRC incorporation which is probably related with the higher Mg concentration. The local spectra obtained from sample B exhibit differences with respect to those of sample A, which suggests that the amount of Mg incorporated into the p-doped shell influences the formation of defects that modify the structure of the DAP band depending on the Mg concentration [32].

A waterfall spectral plot along the main axis of a single nanowire of the annealed sample B lying on a sidewall is shown in Fig. 16. This provides an overall picture of the distribution of the emission bands along the nanowire. While the emission intensity distribution may possibly show variations among the different nanowires, the CL spectral intensity distribution depicted in Fig. 16 is representative of the optical properties of the nanowires along their main axis. The highest DAP emission is detected along the prismatic section and near the base of the pyramidal tip, indicating a high activation of Mg acceptors in these regions, which concurrently show a strong suppression of the YL emission. A significant DAP intensity reduction is detected across the m - r edges in the transition region from the prismatic base to the pyramidal tip. As the tip of the pyramid is approached, the DAP band is strongly quenched while the near-band-edge emission is recovered and a strong YL emission emerges, which may be related to an increase of Ga vacancies close to the apex. The optical activity of the Mg acceptors is also strongly reduced near the base of the nanowire, where a very intense near-band-edge emission is observed, together with the YL emission.

IV. SUMMARY AND CONCLUSIONS

The efficient p-type doping of GaN nanowires requires the control of the Mg flow and post growth annealing. We have studied the CL emission properties of Mg-doped GaN nanowires grown with different Mg/Ga flow ratios. The intensity of the DAP transitions associated with Mg acceptors is enhanced for the lower Mg flows used. When the Mg flow is increased, the CL spectra display a multiline DAP band which cannot be associated with a well-defined DAP transition.

The spectra of semipolar and non-polar faces present different DAP signatures, which indicates the existence of different DAP transitions and hence different Mg incorporation rates. An increase of the Mg/Ga flow ratio results in a lower intensity of the DAP band and in an enhancement of the YL band. The annealing process allows one to increase the intensity of the DAP emission and to reduce that of the YL band at both the semipolar and non-polar faces. The observation of a well-structured DAP band with their corresponding phonon replicas, peaking at the characteristic energy of the DAP transition in Mg-doped GaN, together with the highest DAP /YL intensity ratio observed in annealed nanowires grown with a Mg/Ga flux ratio of 1.4, suggests that these are the most suitable growth conditions regarding the p-type doping efficiency in the studied nanowires. From the CL spectra one can conclude that non-polar faces are suitable for efficient p-type doping with Mg under controlled growth conditions and activation treatments, and that the influence of the m or r face orientation is much lower than that of the Mg flux or the post-growth annealing used.

Even for the highest Mg/Ga flow ratios we have not observed the blue band associated with heavily Mg-doped GaN, neither on the non-polar nor on the semipolar faces analyzed, which suggest that no deep donors have been formed in the studied nanowires. Further studies are required to establish an unambiguous relation between the DAP band

structure and the activation of Mg acceptors. Such a correlation could provide a powerful tool to investigate Mg activation and would enable the determination of the specific growth and annealing conditions for optimizing p-type doping in non-polar and semipolar faces on GaN nanowires.

ACKNOWLEDGMENTS

This work was partially funded by Junta de Castilla y León (VA293U13). We acknowledge the Glo Company for supplying the samples used in this study.

References

- [1] T. Wang, D. Nakagawa M. Lachab, T. Sugahara, and S. Sakai, *Appl. Phys. Lett.* **100**, 261103 (2012).
- [2] S. Li, A. Waag, *J. Appl. Phys.* **111**, 071101 (2012).
- [3] R. Koester, J. S. Hwang, D. Salomon, X. Chen, C. Bougerol, J. P. Barnes, D. L. S. Dang, L. Rigutti, A.de Luna Bugallo, G. Jacopin, M. Tchernycheva, C. Durand, and J. Eymery, *Nano Lett.* **11**, 4839 (2011).
- [4] C. H. Liao, W. M. Chang, Y. F. Yao, H. T. Chen, C. Y. Su, C. Y. Chen, C. Hsieh, H. S. Chen, C. G. Tu, Y. W. Kiang, C. C. Yang, and T. C. Hsu, *J. Appl. Phys.* **113**, 054315 (2013).
- [5] J. R. Riley, S. Padalkar Q. Li, P. Lu, D. D. Koleske, J. J. Wierer, G. T. Wang, and L. J. Lauhon, *Nano Lett.* **13**, 4317 (2013)
- [6] M. D. Kelzenberg, S. W. Boettcher, J. A. Petykiewicz, D. B. Turner-Evans, M. C. Putnam, E. L. Warren, J. M. Spurgeon, R. M. Briggs, N. S. Lewis, and H. A. Atwater, *Nature Materials* **9**, 239 (2010).
- [7] U. Kaufmann, P. Schlotter, H. Obloh, K. Köhler, M. Maier, *Phys.Rev. B* **62**, 10867 (2000).
- [8] B. Monemar, P. P. Paskov, G. Pozina, C. Hemmingsson, J. P. Bergman, T. Kawashima, H. Amano, I. Akasaki, T. Paskova, S. Figge, D. Hommel, and A. Usui, *Phys. Rev. Lett.* **102**, 235501 (2009).
- [9] L. Eckey, U. von Gfug, J. Holst, A. Hoffmann, A. Kaschner, H. Siegle, C. Thomsen, B. Schineller, K. Heime, M. Heuken, O. Schön, and R. Beccard, *J. Appl. Phys.* **84**, 5828 (1998).
- [10] S. C. Cruz, S. Keller, T. E. Mates, U. K. Mishra, and S. P. DenBaars, *J. Cryst. Growth* **311**, 3817 (2009).
- [11] K. Kanaya and S. Okayama, *J. Phys. D* **5**, 43(1972).
- [12] H. Amano, M. Kito, K. Hiramatsu, and I. Akasaki, *Jpn. J. Appl. Phys.* **28**, L2112 (1989).
- [13] T. W. Yeh, Y.T. Lin, B. Ahn, L. S. Stewart, P. D. Dapkus, and S. R. Nutt, *Appl. Phys. Lett.* **100**, 033119 (2012).
- [14] B. Beaumont, S. Haffouz, and P. Gibart, *Appl. Phys. Lett.* **72**, 921 (1998).
- [15] M. Reschikov and H. Morkoc, *J. Appl. Phys.* **97**, 061301 (2005).
- [16] G. Callsen, M. R. Wagner, T. Kure, J. S. Reparaz, M. Bügler, J. Brunmeier, C. Nenstiel, A. Hoffmann, M. Hoffmann, J. Tweedie, Z. Bryan, S. Aygun, R. Kirste, R. Collazo, and Z. Zitar, *Phys. Rev. B* **86**, 075207 (2012).

- [17] M. Reshchikov, J. Xie, L. He, X. Gu, Y. T. Moon, Y. Fu, and H. Morkoc, *Phys. Stat. Sol. c* **2**, 2761 (2005).
- [18] J. Moxom, J. Xu, R. Suzuki, T. Ohdaira, G. Brandes, and J. S. Flynn. *J. Appl. Phys.* **92**, 1898 (2002).
- [19] J. A. Freitas, B. N. Feigelson, T. J. Anderson, *Appl. Phys. Express* **6**, 111001 (2013).
- [20] Y. P. Sui, G. H. Yu, *Chin. Lett.* **28**, 067807 (2011)).
- [21] S. Khromov, C. G. Hemmingsson, H. Amano, B. Monemar, L. Hultman, and G. Pozina, *Phys. Rev. B* **84**, 075324 (2011).
- [22] S. Khromov, B. Monemar, V. Avrutin, X. Li, H. Morkoc, L. Hultman, and G. Pozina, *Appl. Phys. Lett.* **100**, 172108 (2012).
- [23] J. Arbiol, S. Estradé, J. D. Prades, A. Cirera, F. Furtmayr, C. Stark, A. Laufer, M. Stutzmann, M. Eickhoff, M. H. Gass, A. L. Bleloch, F. Peiró, and J. R. Morante, *Nanotechnology* **20**, 145704 (2009).
- [24] T. Remmele, M. Albrecht, K. Irmischer, R. Fornari, M. Straßburg, *Appl. Phys. Lett.* **99**, 141913 (2011).
- [25] F. A. Reboredo, S. T. Pantelides, *Phys. Rev. Lett.* **82**, 1887 (1999).
- [26] G. Pozina, P. P. Paskov, J. P. Bergman, C. Hemmingsson, L. Hultman, B. Monemar, H. Amano, I. Akasaki, and A. Usui, *Appl. Phys. Lett.* **91**, 221901 (2007).
- [27] B. Monemar, *Proc. SPIE* 7939, 7939-07 (2011).
- [28] F. Furtmayr, M. Vilemeyer, M. Stutzmann, A. Laufer, B. K. Meyer, M. Eickhoff, *J. Appl. Phys.* **104**, 074309 (2008).
- [29] J. K. Sheu, Y. K. Su, G. C. Chi, B. J. Pong, C. Y. Chen, C. N. Huang, and W. C. Chen, *J. Appl. Phys.* **84**, 4590 (1998).
- [30] M. W. Bayer, M. S. Brandt, O. Ambacher, M. Stutzmann, E. R. Glaser, R. L. Henry, A. E Wickenden, D. D. Koleske, T. Suski, I. Grzegory, and S. Porowski, *Phys. Rev. B* **16**, 125203 (2001).
- [31] D. Iida, K. Tamura, M. Iwaya, S. Kamiyama, H. Amano, and I. Akasaki, *J. Cryst. Growth* **312**, 3131 (2010).
- [32] A. M. Fischer, S. Srinivasan, F. A. Ponce, B. Monemar, F. Bertram, and J. Christen, *Appl. Phys. Lett.* **93**, 151901 (2008).

TABLES

Sample	Description	p-GaN shell thickness (nm)	Average equivalent diameter (nm)	Average NW Length (nm)
Ref	undoped-GaN NW	none	519	<1000
A	Undoped/p-type GaN core-shell NW structure, Mg/Ga 1.4%	150-200	750	<1100
B	Undoped/p-type GaN core-shell NW structure, Mg/Ga 2.8%	150-200	685	<1200
C	Undoped /p-type GaN core-shell NW structure, Mg/Ga 3.6%	150-200	736	<1300

Table I. Sample characteristics of the GaN/p-GaN core-shell nanowires studied in this work. The samples were grown using trimethyl gallium as a precursor and different Mg/Ga flow ratios.

FIGURES

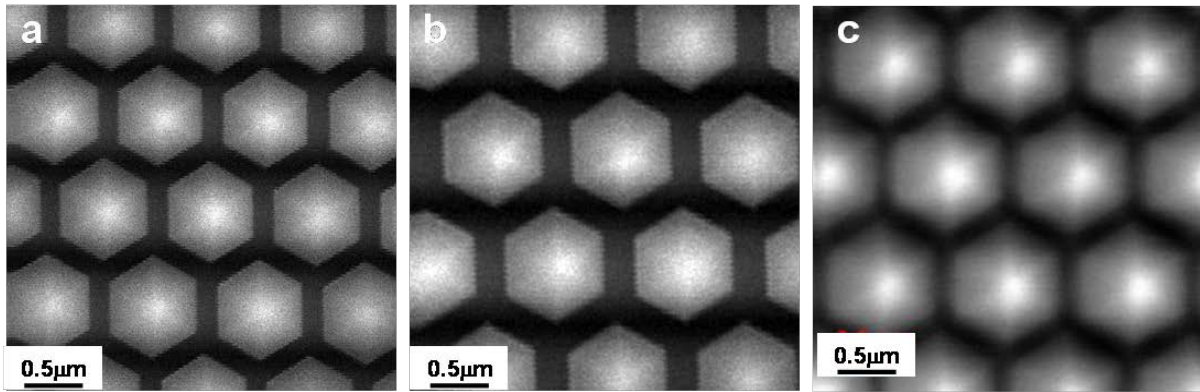


Fig. 1. Top view SEM images of the Mg-doped/undoped GaN nanowires grown with increasing Mg/Ga flow ratios. (a) sample A, Mg/Ga = 1.4%, (b) sample B, Mg/Ga = 2.8%, (c) sample C, Mg/Ga = 3.6%.

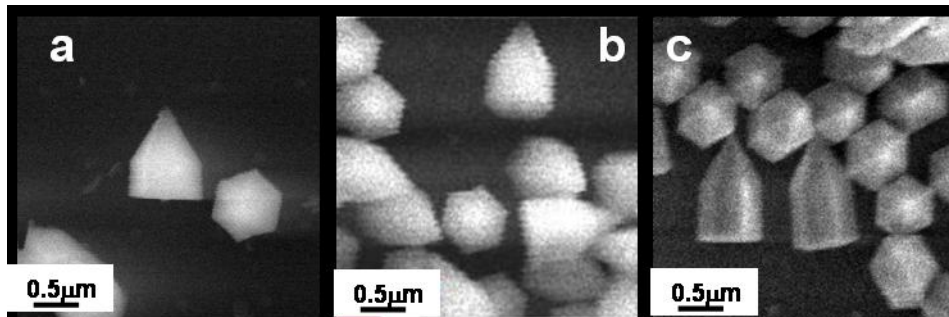


Fig. 2: (a) to (c): side-view SEM images of core-shell GaN nanowires scratched from samples A to C, respectively

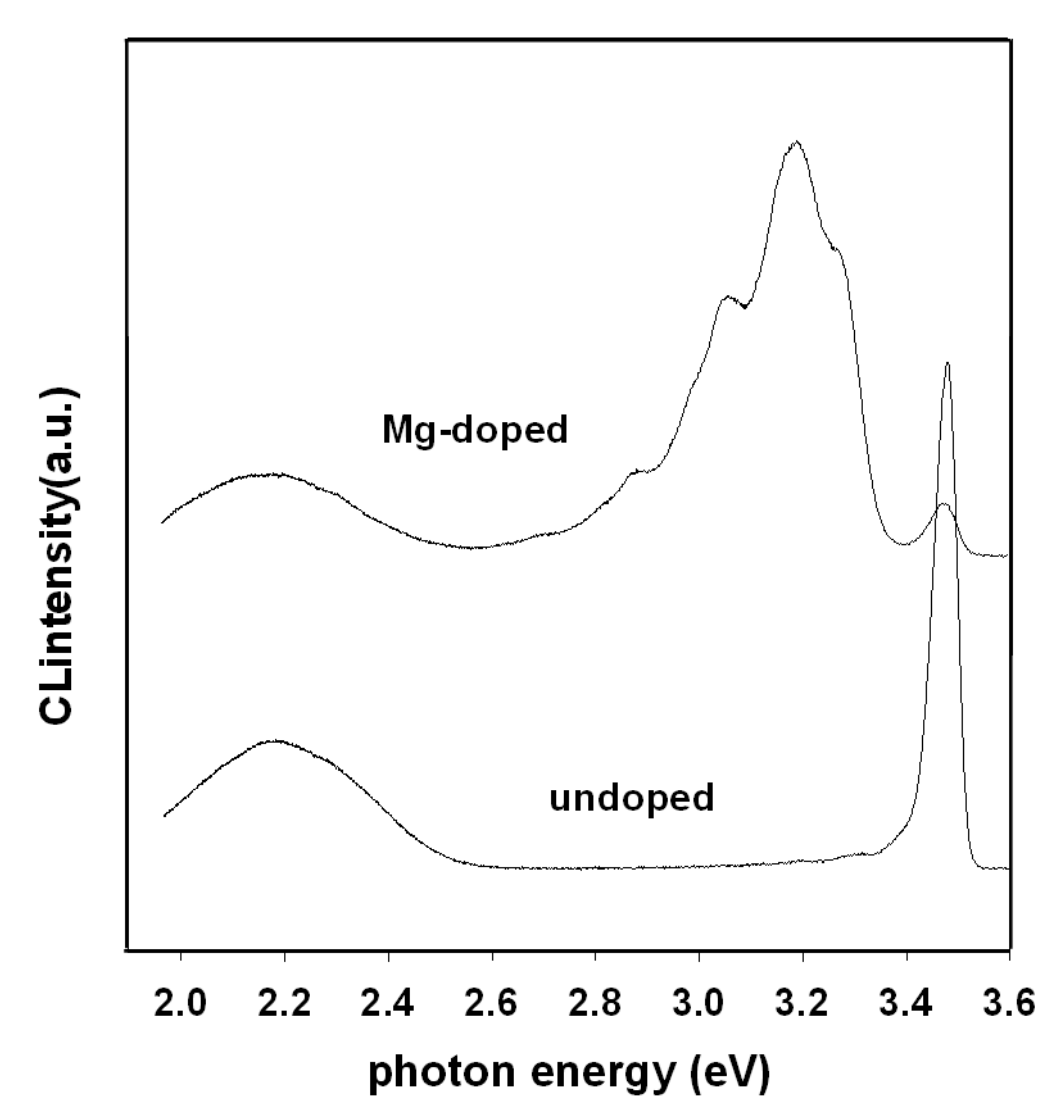


Fig.3. Typical CL spectra at 80 K of Mg-doped and undoped GaN nanowires.

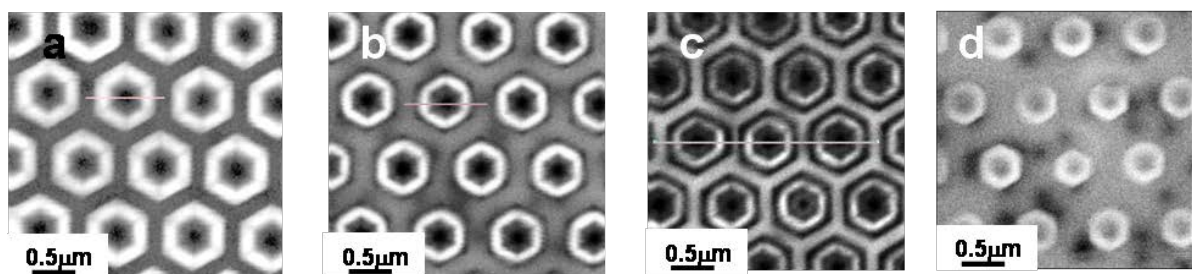


Fig. 4. Top-view panchromatic CL images for different Mg/Ga flow ratios. (a) 1.4%, sample A. (b) 2.8%, sample B. (c) 3.6%, sample C. (d) undoped reference.

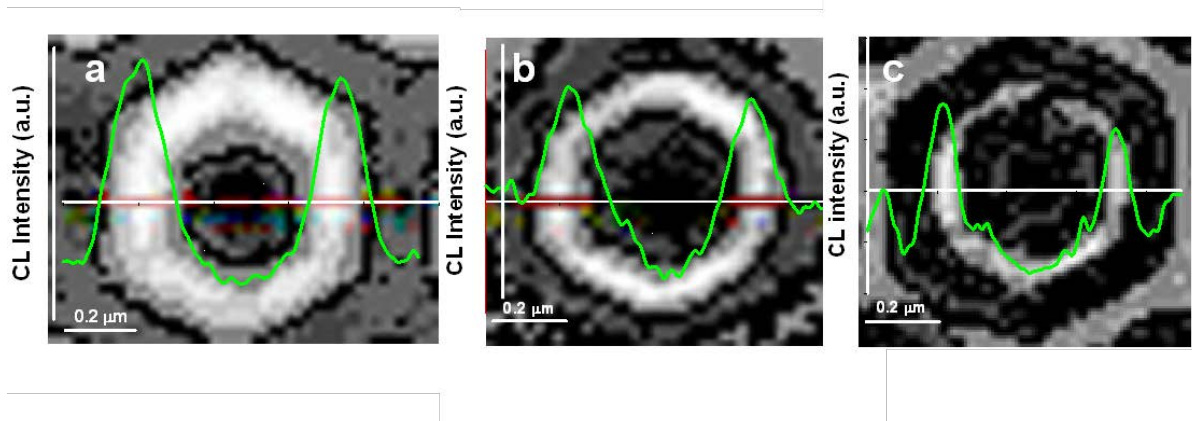


Fig. 5. (a) to (c): top-view CL-intensity scan profiles across the core-shell GaN nanowires for increasing Mg/Ga flow ratio (samples A to C, respectively superimposed to the panchromatic images.

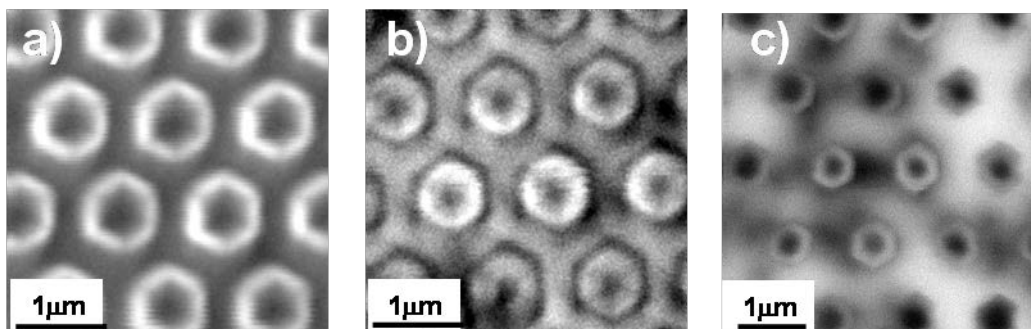


Fig. 6. (a) to (c): respectively, panchromatic CL images of samples A, B after annealing and reference sample.

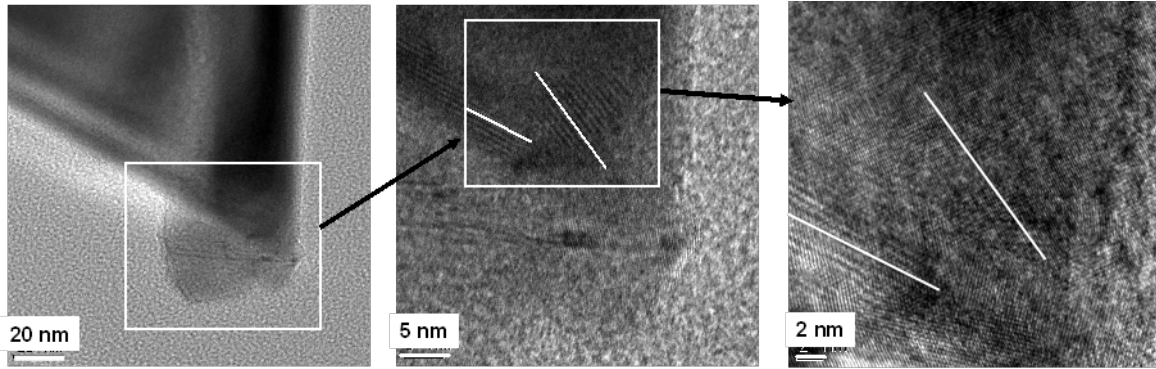


Fig. 7. TEM images at different magnifications of the apex region in sample A, showing the presence of structural defects at the tip.

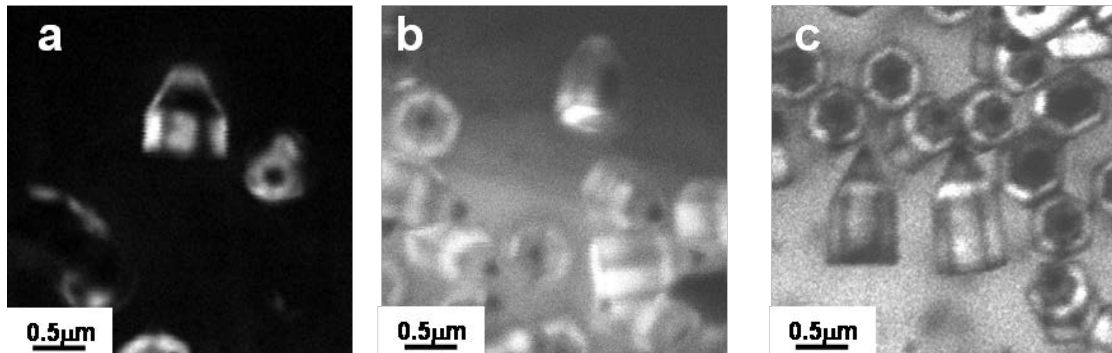


Fig. 8. (a) to (c): Panchromatic CL images of scratched nanowires from samples A to C, respectively, showing the m -plane sidewalls.

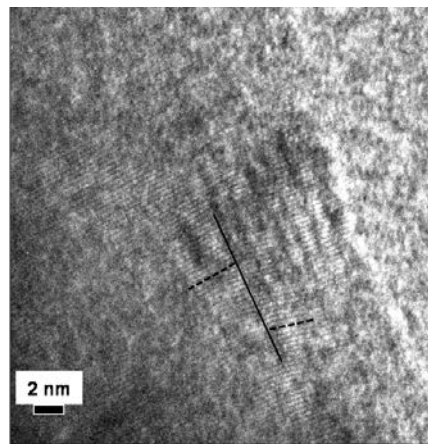


Fig 9. TEM image of the edge region between two m -face prismatic sidewalls in sample C displaying the presence of dislocations.

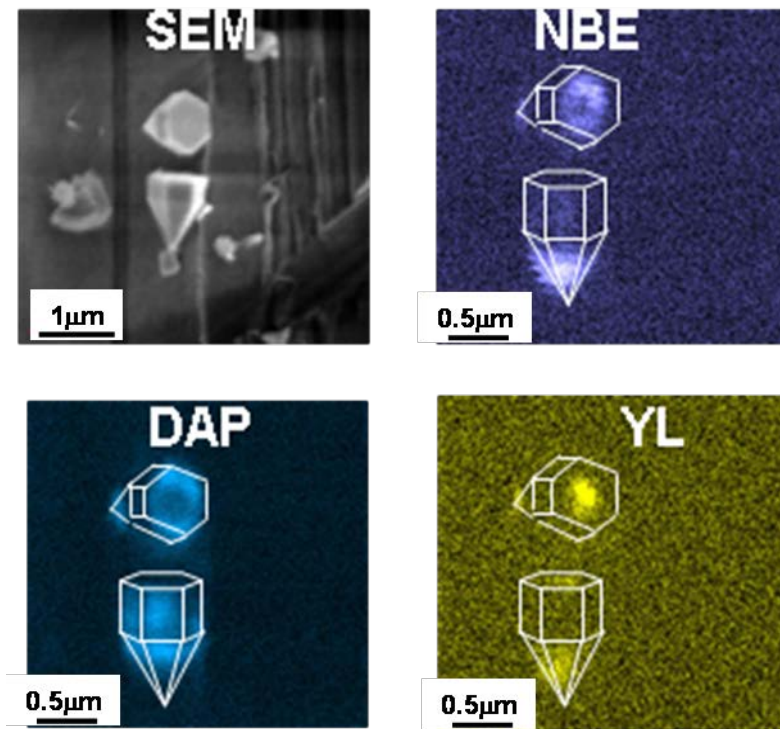


Fig.10. SEM and monochromatic CL images of two nanowires from sample A, revealing the distribution of the different CL emission bands: NBE, DAP and YL band.

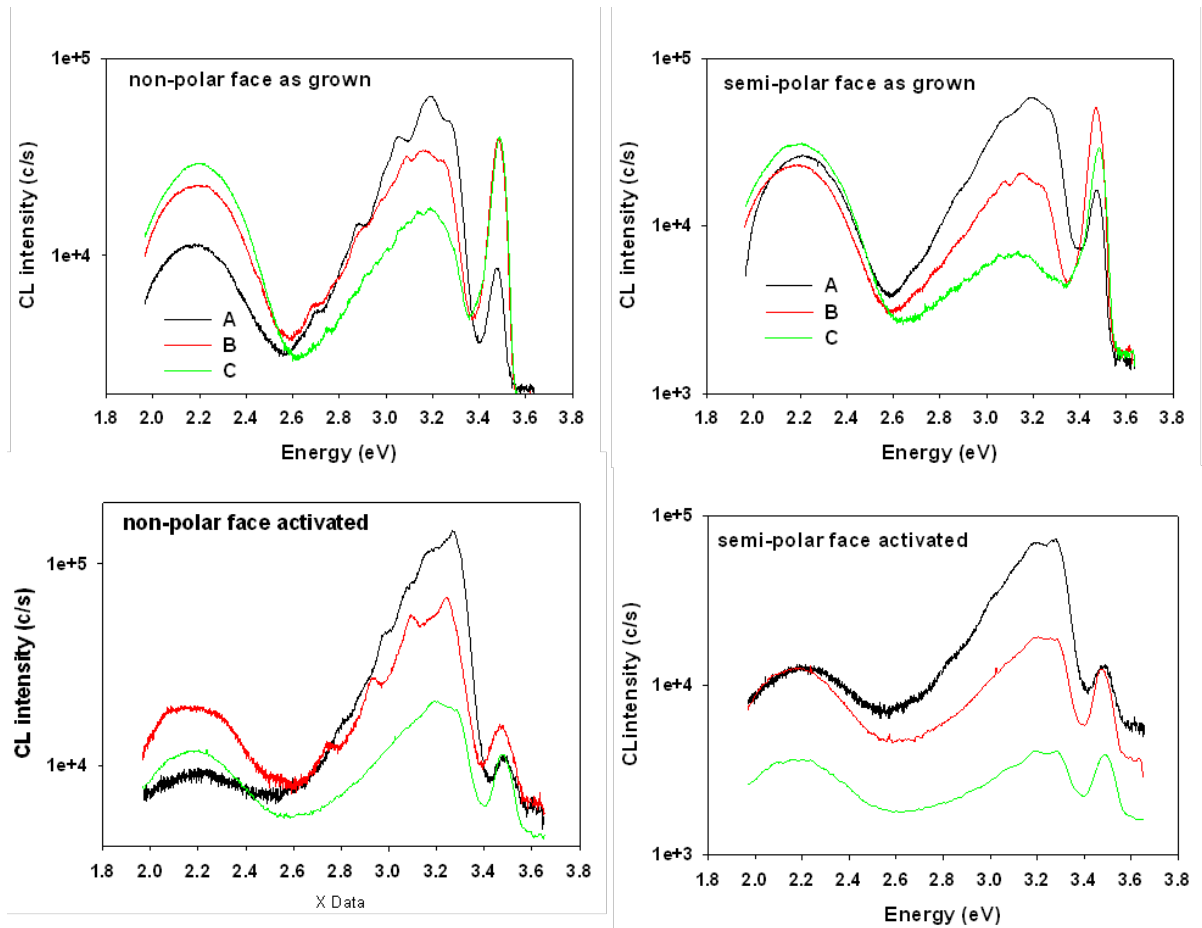


Fig.11. Typical CL spectra obtained from the nanowire samples A, B, and C on different faces. (a) *m* face of the as-grown samples. (b) *r* face of the as-grown samples. (c) *m* face of the annealed samples. (d) *r* face of the annealed samples.

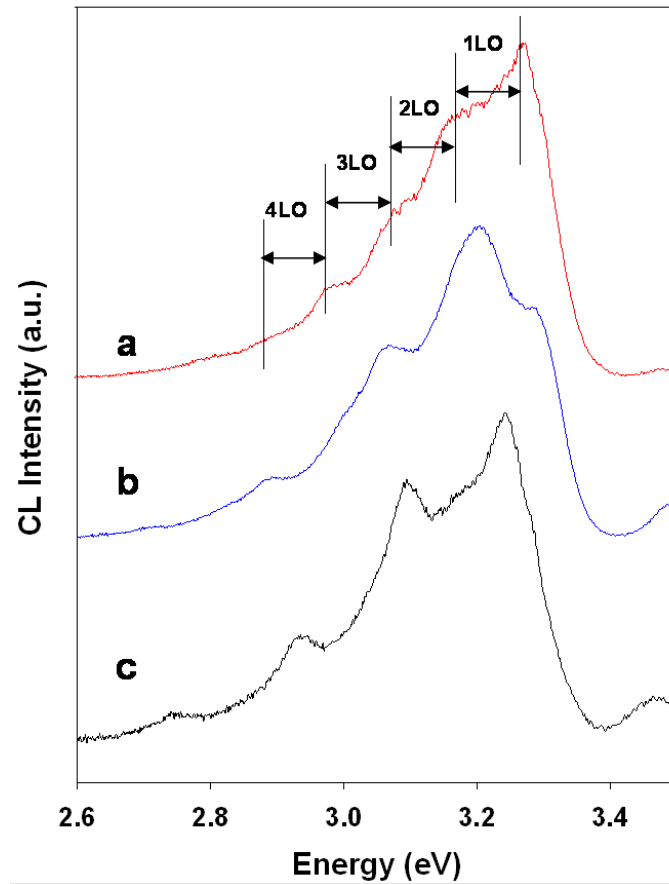


Fig. 12. CL spectra (DAP bands) obtained at 80 K on the *m* faces of annealed sample A (a), on as-grown sample A (b), and on annealed sample B (c).

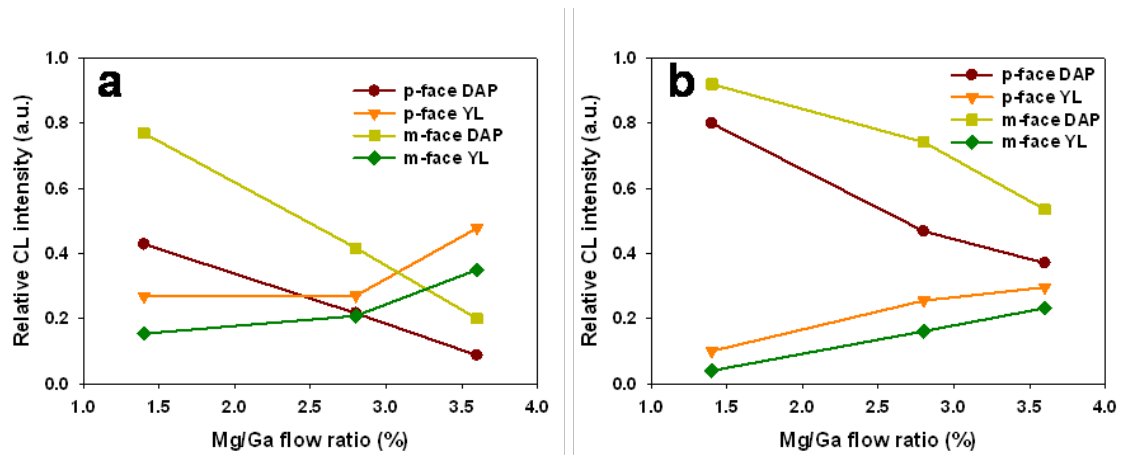


Fig.13. Relative intensities (normalized to the total emission) of the DAP and YL bands in semipolar and non-polar faces as a function of the Mg/Ga flow ratio, before (a) and after annealing (b)

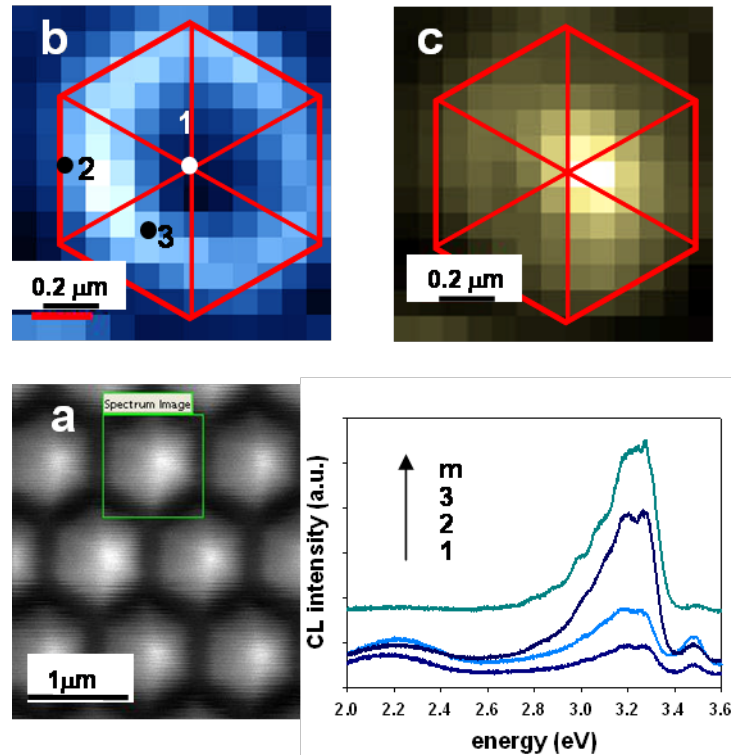


Fig.14. (a) SEM image of the annealed sample A showing the nanowire selected for the study. (b) DAP emission image of the nanowire framed in (a). (c) YL emission image. (d) Local spectra obtained at the locations indicated in (b) compared with the spectrum recorded on the *m*-face.

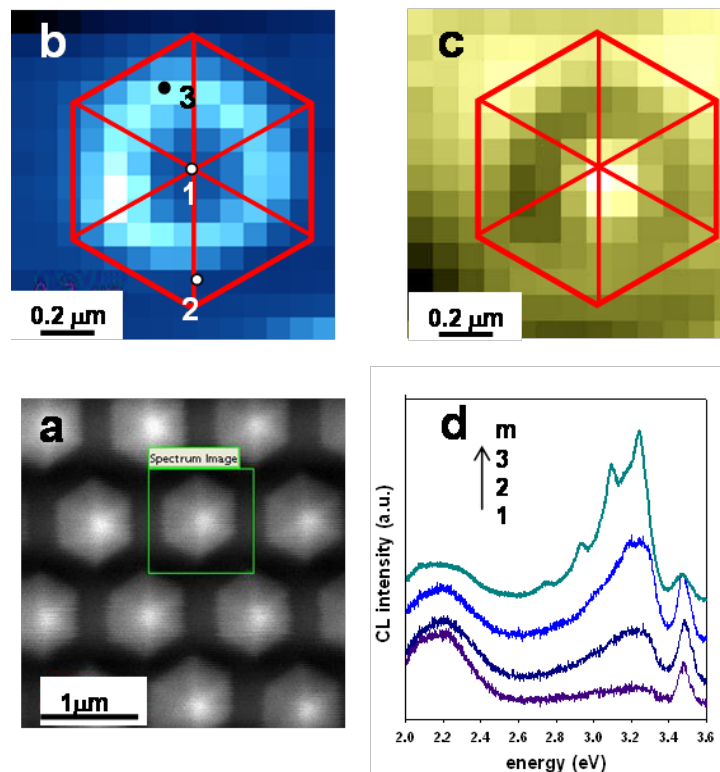


Fig.15. (a) SEM image of the annealed sample B. (b) DAP emission image of the nanowire framed in (a). (c) YL emission image. (d) Local spectra obtained at the locations indicated in (b) compared with the spectrum recorded in the *m*-face.

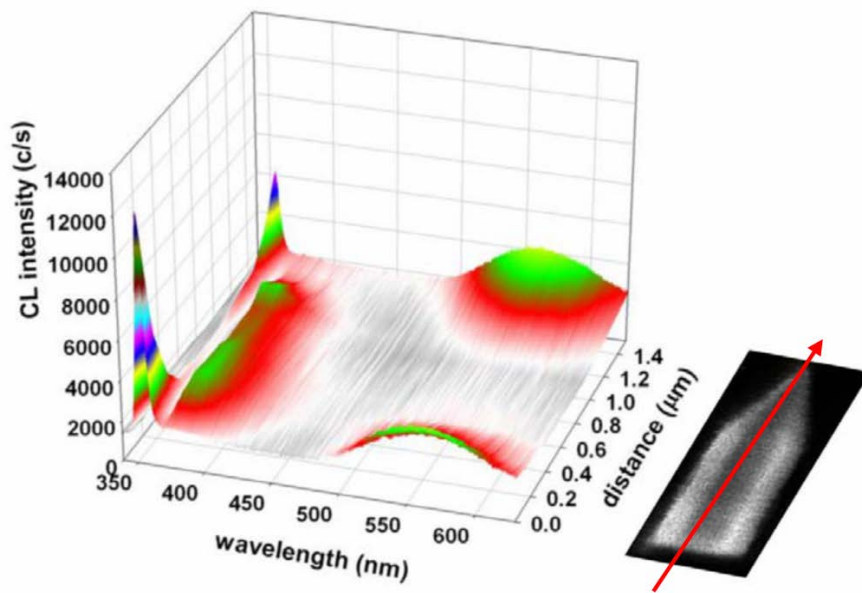


Fig. 16. Waterfall spectral plot showing the spectral distribution of the emission bands along the main axis of a nanowire (annealed sample B).